https://doi.org/10.20965/jrm.2023.p0317

Paper:

Horizontal Fixed Attitude Flight of Quad Rotor Helicopter with Tilting Rotor

Akitaka Imamura

Faculty of Engineering, Osaka Sangyo University
3-1-1 Nakagaito, Daito, Osaka 574-8530, Japan
E-mail: imamura@eic.osaka-sandai.ac.jp
[Received October 16, 2022; accepted January 5, 2023]

A quad rotor helicopter (QRH), a type of unmanned aerial vehicle (UAV), uses a tilted attitude to generate a horizontal thrust component in the flying direction. In the case of autonomous control, the attitude control system is used to tilt the airframe against disturbances such as crosswinds. Consequently, the flying attitude of a QRH is always inclined. In this study, a tilting mechanism for rotors (TMR) was mounted on a QRH to maintain a horizontal attitude. The TMRs were tilted to generate thrust against disturbances without inclining the airframe. The system was constructed using a QRH and TMRs tilted around only one axis and allocated every 90°. Because the airframe is always horizontal, this system can be used for the precise measurement of landforms and buildings. This paper reports the dynamic modeling of QRH equipped with TMRs and discusses the horizontal constant attitude flight using the proposed system.

Keywords: UAV, multi rotor, quad rotor, helicopter, tilt rotor

1. Introduction

Quad rotor helicopters (QRHs), normally called drones, which are used in aerial photography and infrastructure inspections, have been used not only for industrial operations, but also for recreational purposes.

Although safety is the most important factor when operating unmanned aerial vehicles (UAVs), legal and regulatory restrictions are becoming stricter every year because of the increase in serious incidents owing to the increase in the number of users. The risk of the rotor or airframe colliding with surrounding objects is always present, even when sufficient safety precautions are taken, even though multirotor helicopters that employ small-diameter rotors have reduced such risks. In fact, multirotor helicopters, which are equipped with various sensors for attitude control and collision avoidance, have superior flight stability and operability compared with conventional single-rotor helicopters.

In this study, we proposed and compared three control mechanisms with the goal of maintaining the flight attitude of QRHs horizontally under all conceivable situations [1]. The fixed-attitude flight of QRHs achieved by these three methods drastically improves their aerial operability and operational stability. Among the three methods, we proposed the quad tilting rotor helicopter (QTRH) as the mechanism that achieves horizontal fixed-attitude flight with the smallest degree of freedoms (DOFs), and verified it using a prototype [2].

Several studies have been conducted on the tilting mechanism of rotors (TMR) in UAV [3,4]. The Bell Boeing V-22 (Osprey) is a well-known two-rotor aircraft used in practical service. However, many tilt mechanisms operate coaxially in phase with the forward/backward tilt mechanism to switch between rotor blade mode and fixed wing mode.

In the tilt mechanism proposed in this study, the rotor mechanisms mounted on adjacent booms were tilted at a 90° angle relative to each other, employing two degrees of DOFs. Because the objective of a previous study [5–8] was to verify the proposed method, we did not present a theoretical discussion of the relationship between tilt angle and thrust compensation or the dynamic modeling. Therefore, in this study, we present a mathematical model to verify the feasibility of executing a horizontal fixed-attitude flight using a 2-DOF tilt mechanism. Although studies [9–11] that employ mechanisms similar to those employed in this study have been published [2], they focused on tilting the attitude angle by arranging the rotors in plus (+)- [9,10] and H-shaped [11] configurations; thus, they are different from the X-shaped configuration employed in our study and independent. Another study with an objective similar to ours presented sliding mode control using an observer [12].

2. Quad Tilting Rotor Helicopter

2.1. Tilting Method

In aerial photography, the tilting of the airframe causes the image to be captured in a tilted state. To prevent this, the camera is mounted on a gimbal and tilted in the reverse direction to counteract the airframe tilt. In this research, a tilt-rotor mechanism is used instead of a gimbal mechanism, but it plays a different role. By tilting the rotor

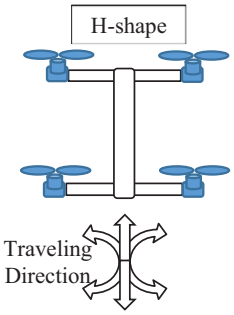

Fig. 1. H-shape QTRH.

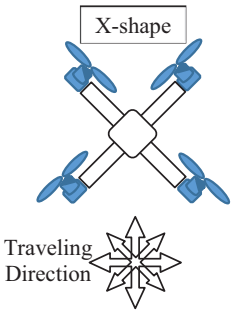

Fig. 2. X-shape QTRH.

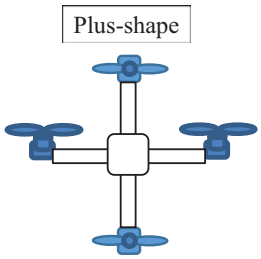

Fig. 3. Plus-shape QTRH.

thrust, the aircraft can fly in a desired direction without tilting its attitude.

Generally, QRHs use a fixed pitch rotor, making it easy to apply TMR for thrust tilt. There are three frame configurations for QTRHs, in which the four rotors are simultaneously tilted, all of which require two additional DOFs. In the H-shape shown in **Fig. 1**, the rotors on the left and right sides are tilted at the same angle [11]. Although there is no thrust loss, the direction of movement is limited. In the X-shape, as shown in **Fig. 2**, the diagonally placed rotors are tilted to the same angle. The thrust is the vector resultant of the individual rotor thrusts, which involves cancellation components and results in a maximum loss factor of $\sqrt{2}/2$. However, there is no limit to the direction of movement; omnidirectionally uniform thrust can be obtained, and lift loss does not occur. Thus, we employed an X-shaped configuration for the QTRH used in this study. The plus-shape shown in **Fig. 3** was obtained by rotating the X-shape by 45°. As they are unstable in terms of pitch and roll during steering, they are rarely employed in current QRHs.

An X-shape can be created to perform translations with two additional DOFs by tilting the two rotors on the same axis in the same phase. It is possible, by adding four DOFs, to tilt the two coaxial rotors in reverse phase to execute rotations. However, conventional yaw control can be used to perform rotation; therefore, this study added only two DOFs to tilt the thrust.

The X-shaped QTRH is capable of functioning under crosswinds and other disturbances, and presents a small projection area to the wind compared to conventional QTRHs, which make it easy to maintain a horizontal attitude (**Fig. 4**).

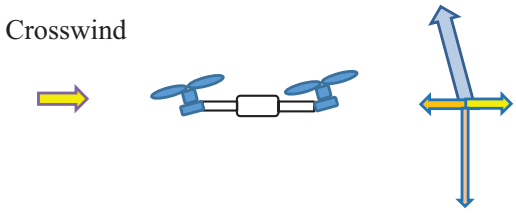

Fig. 4. QTRH under crosswind.

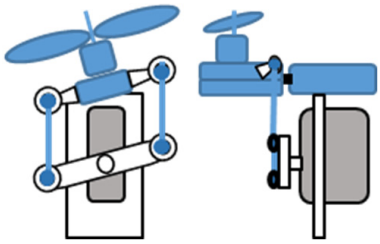

Fig. 5. Structure of TMR.

Fig. 6. Assembled TMR.

2.2. Tilting Rotor Mechanism

Although TMR can be configured using two DOFs, we used four servo-motor-and-parallel-link sets to simplify the mechanism (**Figs. 5** and **6**). To operate the QTRH, the radio-control transmitter sent two signal channels (two DOFs: forward-backward and left-right), each of which was split into two channels by the receiver to drive the four servomotors. Because thrust loss can occur when there are phase errors between individual TMRs, accurate phase adjustment of the TMRs was necessary to control the QTRH. The maximum tilt angle of the experiment model was $\pm 40°$ due to the limitation of the TMR link mechanism, and the QTRH attained peak speed at these tilt angles. The thrust tilt angle, which was the vector resulting from the TMRs, was equal to the airframe tilt angle in conventional flights.

The skid effect obtained by the TMRs represented the horizontal-component thrust, whereas the vertical component represented the lift.

The TMRs tilted the thrust of each rotor separately, such that their resultant vector determined the direction

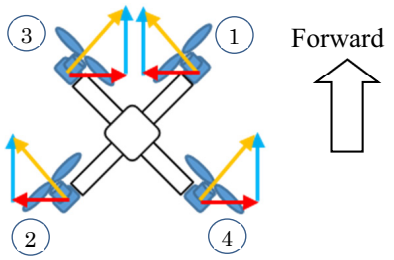

Fig. 7. Motion by vector composition of TMR (anti-phase).

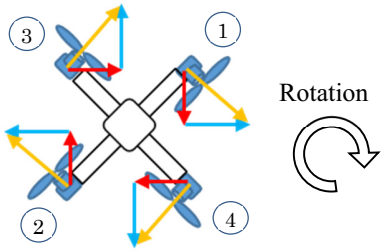

Fig. 8. Motion by vector composition of TMR (in-phase).

of the forward flight, as shown in **Fig. 7**. Furthermore, the QTHR exhibited robustness against external disturbances, whereas the use of the TMRs resulted in the following losses:

- Increase of airframe weight
- Complex mechanism and control
- Reduction of lift and partial cancellation of thrust due to rotor tilt

Of these, weight gain is the most important. However, this increase can be considered minimal when compared to the other two methods [13, 14], which employ more complex mechanisms to achieve results similar to those of TMRs.

Two tilt control strategies, involving coaxial rotors, can be considered for the TMRs, resulting in different effects of the thrust tilt.

- Anti-phase (**Fig. 7**, skid effect, linear movement)
- In-phase (**Fig. 8**, yaw effect, rotation)

In this study, we prototyped an experimental model in which the anti-phase mode was used as the default control of the TMRs, and used it to carry out flight tests. The skid effect of the TMRs was achieved by the QTRH's functions to maintain its attitude and altitude. The operator drove the four TMRs using two-axis control on the radio-control transmitter to tilt the thrust in the desired direction.

3. Tilt Angle and Thrust Compensation

The tilt angles of the TMRs consisted of 2-DOF tilt angles, which were determined based on the desired direction of movement and speed. When the speed was constant, the 2-DOF tilt angles were determined using trigonometric functions, where the magnitude of the resultant vector was constant. The higher the desired speed, the larger was the tilt angle, where the thrust loss could no longer be ignored.

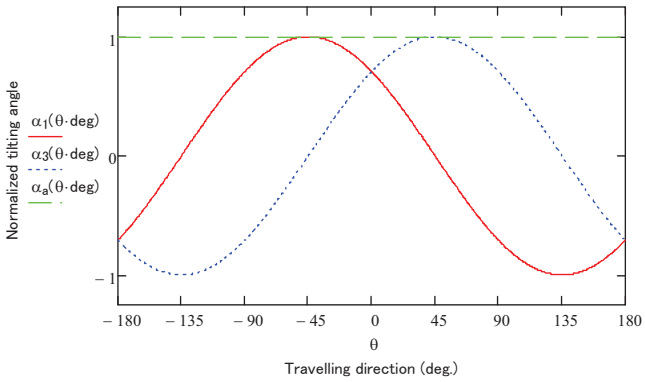

Fig. 9. Normalized tilting angle vs. traveling direction.

3.1. Variation of Tilt Angle

As the TMR tilt angles consisted of 2-DOF orthogonal components, they are expressed as vectors using complex numbers.

$$\alpha(\theta) = a \cdot e^{j\left(\theta+\frac{\pi}{4}\right)}, \quad \ldots\ldots\ldots\ldots \quad (1)$$

where α and θ are the tilt and steering angles, respectively. When $a = 1$, the tilt angle is called the normalized tilt angle.

$\alpha_1(\theta)$ is the normalized tilt angle of axis 1 (rotors Nos. 1 and 2), $\alpha_3(\theta)$ is the normalized tilt angle of axis 2 (rotors Nos. 3 and 4), and $\alpha_a(\theta)$ is the magnitude of the tilt angle.

$$\alpha_1(\theta) = \mathrm{Re}[\alpha(\theta)], \quad \ldots\ldots\ldots\ldots \quad (2)$$
$$\alpha_3(\theta) = \mathrm{Im}[\alpha(\theta)], \quad \ldots\ldots\ldots\ldots \quad (3)$$
$$\alpha_a(\theta) = |\alpha(\theta)| = a. \quad \ldots\ldots\ldots\ldots \quad (4)$$

The magnitude of the tilt angle was determined by the thrust; therefore, it remained constant when the thrust was constant. Furthermore, because the orthogonal components of the two axes varied depending on the traveling direction, the normalized tilt angles were represented using trigonometric functions (**Fig. 9**).

The normalized tilt angle of axis 1 was ± 1 (maximum) when the airframe moved diagonally at angles of $-45°$ and $135°$, when the normalized tilt angle of axis 2 was zero (neutral). Similarly, when moving at angles of $45°$ and $-135°$, axis 1 was zero and axis 2 was ± 1. When the airframe traveled in the directions $0°$ and $\pm 180°$ (forward and backward) and $-90°$ and $90°$ (left and right), the normalized tilt angles of both axes were $\sqrt{2}/2$. The rotor thrust T necessary for flight at this time was determined from the airframe weight w, as follows:

$$T = \frac{w}{\cos(a)}. \quad \ldots\ldots\ldots\ldots \quad (5)$$

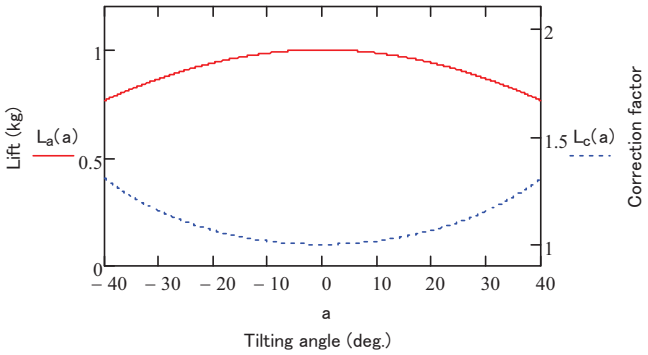

Fig. 10. Lift and correction factor vs. traveling direction.

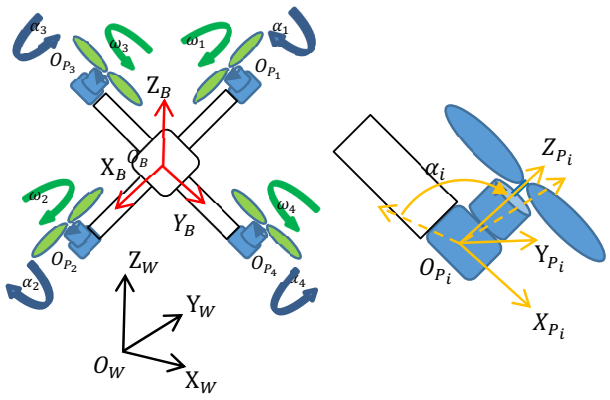

Fig. 11. Three coordinate systems.

The drag and lift were computed using Eqs. (6) and (7), respectively.

$$D(a) = T\sin(a)\cdot e^{j\left(\theta+\frac{\pi}{4}\right)}, \quad \ldots\ldots\ldots \quad (6)$$

$$L(a) = T\cos(a)\cdot e^{j\left(\theta+\frac{\pi}{4}\right)}, \quad \ldots\ldots\ldots \quad (7)$$

$$L_a(a) = |L(\theta)|. \quad \ldots\ldots\ldots\ldots \quad (8)$$

3.2. Variation of Thrust Compensation Factor

Although thrust was obtained from the rotor tilt angles, it also produced lift losses. The rotor thrust was compensated to maintain the altitude. The compensation factor was computed by substituting $\theta = 0$ and $T = w$ into Eq. (7), as follows:

$$L_c(a) = \frac{w}{|L(a)|}. \quad \ldots\ldots\ldots\ldots \quad (9)$$

Because the maximum tilt angle of the experimental model was $\pm 40°$, the maximum compensation factor was $L_c(\pm 40°) = 1.305$. Because the rotor thrust was proportional to the square of the rotational speed [15], the rotational speed was increased by $1.305^2 = 1.703$, or approximately 1.7 times, to perform this compensation. The same "proportional to the squared value" relation was also applied to Eqs. (16) and (32) discussed later. **Fig. 10** shows the variations of lift and compensation factors with the tilt angle when thrust T was assumed equal to 1 kg.

4. Modeling

4.1. Three Types of Coordinate Systems

This study employed three coordinate systems similar to those in [3] (**Fig. 11**).

- Inertial coordinate system F_w: $(O_w; X_w, Y_w, Z_w)$; O_w: origin at the ground surface.
- Airframe coordinate system F_B: $(O_B; X_B, Y_B, Z_B)$; O_B: origin at the airframe (center of gravity).
- Rotor coordinate system F_{P_i}: $(O_{P_i}; X_{P_i}, Y_{P_i}, Z_{P_i})$ $(i = 1,\ldots,4)$; O_{P_i}: origin of i-th rotor system (center of tilt).

We now define the rotation matrices to perform transformations between these coordinate systems. Normally, the transformation from coordinate system 1 to coordinate system 2 is expressed as ${}^2R_1 \in SO(3)$, where $SO(3)$ represents a rotation matrix in three dimensions. Therefore, we used the following notations:

- ${}^WR_B$: transformation of origin of airframe coordinate system to inertial coordinate system,
- ${}^BR_{P_i}$: transformation of origin of i-th-rotor coordinate system to airframe coordinate system,

where ${}^WR_B$ is written accurately as follows:

$${}^WR_B = \begin{bmatrix} \cos\psi\cos\theta & \cos\psi\sin\theta\sin\phi - \sin\psi\cos\phi & \cos\psi\sin\theta\cos\phi + \sin\psi\sin\phi \\ \sin\psi\cos\theta & \sin\psi\sin\theta\sin\phi + \cos\psi\cos\phi & \sin\psi\sin\theta\cos\phi - \cos\psi\sin\phi \\ -\sin\theta & \cos\theta\sin\phi & \cos\theta\cos\phi \end{bmatrix}, \quad \ldots \quad (10)$$

where ϕ, ψ, and θ represent rotations around the X_B, Y_B, and Z_B axes, or roll, pitch, and yaw, respectively, which were used to represent the operations and movements of the airframe. The tilt angles of the TMRs are expressed as

- $\alpha_1 = -\alpha_2$: tilt angle of axis 1, rotation angle around X_{P_1} and X_{P_2} axes,
- $\alpha_3 = -\alpha_4$: tilt angle of axis 2, rotation angle around X_{P_3} and X_{P_4} axes.

As the two coaxial TMRs tilted synchronously in the system used in this study, we assumed that the two orthogonal axes rotated. However, the tilt angles of the two coaxial rotor coordinate systems had opposite signs because they were rotationally symmetric.

The coordinate transformation from the rotor to the airframe coordinate system, in which the tilt angle of the i-th rotor rotated about the X_{P_i} axis and the rotors were arranged at 90° angle intervals around Z axis, is expressed as

$${}^BR_{P_i} = R_Z\left((i-1)\frac{\pi}{2}\right)R_X(\alpha_i), \quad i = 1,\ldots,4. \quad (11)$$

Similarly, the origin of the i-th rotor system when the rotors were rotationally arranged at 90° intervals at a boom length L from the airframe center $P = {}^{B}O_{P_i} \in \mathbb{R}^3$ is expressed as follows:

$$ {}^{B}O_{P_i} = R_Z\left((i-1)\frac{\pi}{2}\right)\begin{bmatrix} L \\ 0 \\ 0 \end{bmatrix}, \quad i = 1, \ldots, 4 \quad . \quad . \ (12) $$

where $R_X(\theta)$, $R_Y(\theta)$, and $R_Z(\theta)$ represent the rotation matrices around the X, Y, and Z axes, respectively. $\omega_B \in \mathbb{R}^3$ denotes the angular velocity of the airframe and ω_i is the (rotational) speed of the i-th rotor, which is around the Z_{P_i} axis.

4.2. Dynamic Model

The equations of motion were determined based on [a] and [3]. To derive the equations of motion using Newton's method, two equations were required: one for translation and the other for rotation. The basic form of the equation of motion for translation is

$$ m\ddot{x} = F, \quad . . . . (13) $$

where x is the airframe position, m is the mass, and F is the force acting on the airframe. The basic form of the equation of motion for rotation is

$$ J\ddot{\theta} = M, \quad . . . . (14) $$

where θ is the airframe attitude angle, J is the moment of inertia, and M is the moment acting on the airframe.

4.2.1. Equation for Translational Motion

The equation for translational motion for a conventional QRH in an inertial coordinate system is given by

$$ m\begin{bmatrix} \ddot{x} \\ \ddot{y} \\ \ddot{z} \end{bmatrix} = \begin{bmatrix} 0 \\ 0 \\ -mg \end{bmatrix} + {}^{W}R_B F_T + F_D, \quad . . . . . (15) $$

where the first term on the right-hand side is related to gravity, the second term is the thrust, and the third term is the aerodynamic drag. The thrust F_T acting on the airframe was determined from the four rotor speeds, as follows:

$$ F_T = \begin{bmatrix} 0 \\ 0 \\ C_L \sum_{i=1}^{4} {\omega_i}^2 \end{bmatrix}, \quad . . . . (16) $$

where C_L denotes the lift coefficient generated by the rotors and ω_i is the angular velocity of the i-th rotor. The sum of the lifts generated by the four rotors was the thrust acting on the airframe. The aerodynamic drag F_D is given by

$$ F_D = -\mu\begin{bmatrix} \dot{x} \\ \dot{y} \\ \dot{z} \end{bmatrix} - \kappa\begin{bmatrix} \dot{x} \\ \dot{y} \\ \dot{z} \end{bmatrix}^2, \quad . . . . (17) $$

where the first term represents the viscous drag, in which μ is the coefficient of viscous drag (air friction), and the second term represents inertial drag. The coefficient κ is described as

$$ \kappa = \frac{1}{2}C_D \rho S, \quad . . . . (18) $$

where S is the front projection area, ρ is the air density, and C_D is the drag coefficient attributed to the airframe shape.

For the experimental model in this study, the normal mode is described by the equation for translational motion (Eq. (15)). Because S varied depending on attitude changes in the normal mode, F_D varied with speed and κ.

Subsequently, for the skid mode, in which the TMRs are used to perform thrust vectoring, we assumed that the centers of gravity of the rotor systems P_i lie at their respective origins O_{P_i} for simplicity. This allowed us to ignore the inertial effects on the rotor systems owing to the acceleration of the quad rotor airframe in space. Thus, the position $\mathrm{P} = {}^{W}O_B$ of the quad rotor airframe in the inertial coordinate system is described in a manner similar to Eq. (15), as follows:

$$ m\ddot{p} = m\begin{bmatrix} 0 \\ 0 \\ -g \end{bmatrix} + {}^{W}R_B \sum_{i=1}^{4} {}^{B}R_{P_i} T_{P_i} + F_D. \quad . . . (19) $$

Because there was no attitude change in the skid mode, S remained constant at its minimum value; therefore, F_D varied only with speed. m is the total weight of the quadcopter airframe and rotor systems, g is the acceleration due to gravity, and T_{P_i} is the moment around the motor axes, which is described later.

4.2.2. Equation for Rotational Motion

The equation for the rotational motion of a conventional QRH in the airframe coordinate system is expressed as

$$ J\dot{\omega} + \omega \times (J\omega) = \tau - \tau_D, \quad . . . . (20) $$

where ω is the angular velocity of the airframe attitude.

Because the base vectors varied with time when the coordinate system was rotated, as in the case of the airframe coordinate system, they could be differentiated as expressed by the second term on the left-hand side.

The first term, τ, on the right-hand side of Eq. (20) is the torque generated by the rotors, and is determined by its components around the respective axes.

$$ \tau_x = LC_L \sin\beta\left({\omega_1}^2 + {\omega_2}^2 - {\omega_3}^2 - {\omega_4}^2\right), \quad . \quad (21) $$

$$ \tau_y = LC_L \cos\beta\left(-{\omega_1}^2 + {\omega_2}^2 + {\omega_3}^2 - {\omega_4}^2\right), \quad (22) $$

$$ \tau_z = C_{DR}\left(-{\omega_1}^2 + {\omega_2}^2 - {\omega_3}^2 + {\omega_4}^2\right), \ . \ . \ . \quad (23) $$

where L is the distance from the center of gravity of the

quadcopter to the motor, C_L is the rotor lift coefficient, and C_{DR} is the rotor drag coefficient. The second term, τ_D, on the right-hand side of Eq. (20) is the drag generated by the viscosity of air, and is proportional to the airframe's angular velocity, as follows:

$$\tau_D = -\mu \begin{bmatrix} \omega_x \\ \omega_y \\ \omega_z \end{bmatrix} \quad \ldots\ldots\ldots\ldots\ldots (24)$$

J is the moment of inertia and is described by a diagonal matrix because the quadcopter is symmetric in the left-right and fore-aft directions, as follows:

$$J = \begin{bmatrix} J_{xx} & 0 & 0 \\ 0 & J_{yy} & 0 \\ 0 & 0 & J_{zz} \end{bmatrix} \quad \ldots\ldots\ldots\ldots\ldots (25)$$

Substituting Eqs. (21)–(25) into Eq. (20), we obtained

$$\begin{bmatrix} J_{xx} & 0 & 0 \\ 0 & J_{yy} & 0 \\ 0 & 0 & J_{zz} \end{bmatrix} \begin{bmatrix} \dot{\omega}_x \\ \dot{\omega}_y \\ \dot{\omega}_z \end{bmatrix} = \begin{bmatrix} \tau_x \\ \tau_y \\ \tau_z \end{bmatrix} - \mu \begin{bmatrix} \omega_x \\ \omega_y \\ \omega_z \end{bmatrix} + \begin{bmatrix} (J_{yy} - J_{zz})\,\omega_y\omega_z \\ (J_{zz} - J_{xx})\,\omega_x\omega_z \\ (J_{xx} - J_{yy})\,\omega_x\omega_y \end{bmatrix} \quad \ldots (26)$$

In the experimental model used in this study, the normal mode was expressed by the rotational motion equation.

In the case of the skid mode, where the TMRs executed thrust vectoring, the angular velocities of the rotors are described as

$$\omega_{P_i} = {}^B R_{P_i}^T \omega_B + \begin{bmatrix} \dot{\alpha}_i & 0 & \bar{\omega}_i \end{bmatrix}^T, \quad \ldots\ldots\ldots (27)$$

where $\omega_B \in \mathbb{R}^3$ denotes the angular velocity of the airframe and $\bar{\omega}_i \in \mathbb{R}$ is the rotor speed (angular velocity) around the Z_{P_i} axis. Thus, the angular acceleration is described as

$$\dot{\omega}_{P_i} = {}^B R_{P_i}^T \dot{\omega}_B + {}^B \dot{R}_{P_i}^T \omega_B + \begin{bmatrix} \ddot{\alpha}_i & 0 & \dot{\bar{\omega}}_i \end{bmatrix}^T. \quad \ldots (28)$$

The torque created by the respective rotor systems, expressed in Euler angles, is expressed as:

$$\tau_{P_i} = I_{P_i}\dot{\omega}_i + \omega_{P_i} \times I_{P_i}\omega_{P_i} - \tau_{ent_i}, \quad \ldots\ldots\ldots (29)$$

where $I_{P_i}\omega_{P_i} \in \mathbb{R}^{3\times 3}$ is the moment of inertia of the rotor systems and is expressed by a positive diagonal matrix. τ_{ent_i} is the external torque acting on the rotor systems. In this study, the rotary anti-torque acting on the Z_{P_i} axis owing to aerodynamic drag was modeled as

$$\tau_{ent_i} = \begin{bmatrix} 0 & 0 & -k_m \omega_{P_{i_Z}} \left| \omega_{P_{i_Z}} \right| \end{bmatrix}^T, \quad k_m > 0. \quad \ldots (30)$$

Thus, the equation for rotational motion of the quadcopter airframe B and the four rotors P_i is as follows:

$$\tau_B = I_B\dot{\omega}_B + \omega_B \times I_B\omega_B + \sum_{i=1}^{4} {}^B R_{P_i} T_{P_i}, \quad \ldots\ldots (31)$$

where $I_B \in \mathbb{R}^{3\times 3}$ is the airframe's moment of inertia, expressed using a positive diagonal matrix, and $\tau_B \in \mathbb{R}^3$ is the external torque acting on the airframe B. Expressing the four moments caused by rotor thrust around the Z_{P_i} axis as follows:

$$T_{P_i} = \begin{bmatrix} 0 & 0 & k_f \bar{\omega}_i \left| \bar{\omega}_i \right| \end{bmatrix}^T, \quad k_f > 0, \quad \ldots\ldots (32)$$

the equation of rotational motion (Eq. (31)) could then be written, using the origin ${}^B O_{P_i}$ of the airframe coordinate system (the anti-torque of the rotors is already given by τ_{P_i}), as follows:

$$\tau_B = \sum_{i=1}^{4} \left({}^B O_{P_i} \times {}^B R_{P_i} T_{P_i} \right). \quad \ldots\ldots\ldots (33)$$

The equations for translation and rotation of the QTRH were modeled using Eqs. (19) and (33), respectively. The torque $\tau_{\alpha_{1_i}} = (\tau_{1_i})^T \in \mathbb{R}$ around the X_{P_i} axis, which tilted the rotor, and the rotor torque $\tau_{\bar{\omega}_i} = (\tau_{P_i})^T Z_{P_i} \in \mathbb{R}$ generated around the X_{P_i} axis were inputted.

4.2.3. Kinematic Equation

The attitude angles (ϕ, θ, and ψ) in the inertial coordinate system cannot be determined from the equation of rotational motion, which is expressed in the airframe coordinate system. The airframe Euler angles can be determined by transforming the angular velocity ω in the airframe coordinate system to the inertial coordinate system. The coordinate transformation

$$\begin{bmatrix} \dot{\phi} \\ \dot{\theta} \\ \dot{\psi} \end{bmatrix} = \begin{bmatrix} 1 & \sin\phi\tan\theta & \cos\phi\tan\theta \\ 0 & \cos\phi & -\sin\phi \\ 0 & \dfrac{\sin\phi}{\cos\phi} & \dfrac{\cos\phi}{\cos\theta} \end{bmatrix} \begin{bmatrix} \omega_x \\ \omega_y \\ \omega_z \end{bmatrix}, \quad \ldots (34)$$

yields the attitude angles, and is called the kinematic equation.

4.3. Control System

In this study, we employed proportional-integral-derivative (PID) control, which is a basic function of the flight controller, to maintain altitude and attitude in skid mode. A block diagram of the skid mode is shown in **Fig. 12**.

5. Experiment Model

Although the experimental model was previously described in [1, 2], we describe it here along with the updated information.

5.1. Specifications of Experiment Model

The QTRH had a simple X-shaped frame structure (**Fig. 2**) that allowed for omnidirectional movement. A photograph of the experimental model is shown in **Fig. 13** and its specifications are listed in **Tables 1** and **2**.

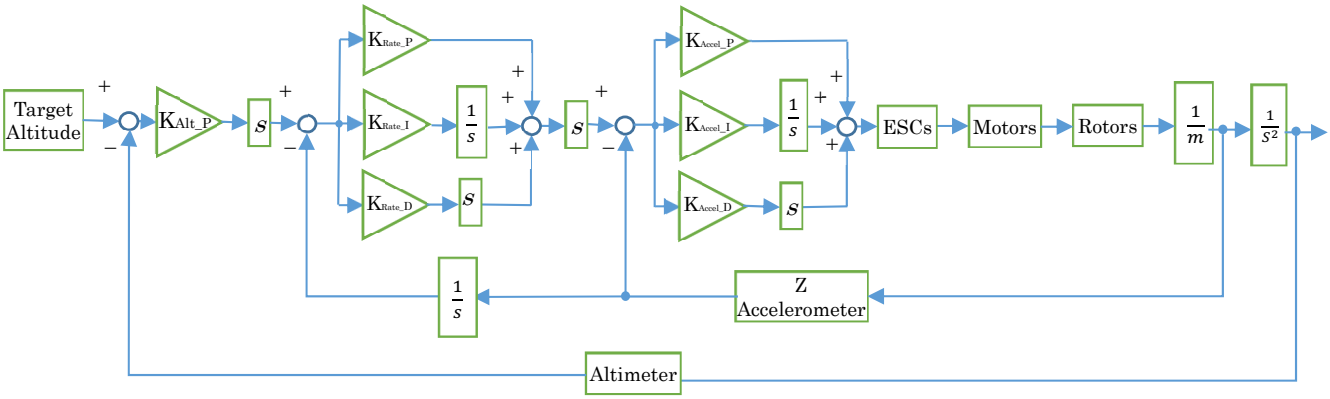

Fig. 12. Altitude and attitude hold functions in the skid mode.

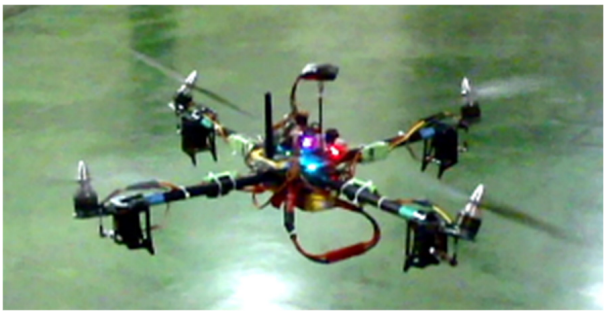

Fig. 13. Experimental setup of TMR-equipped QTRH.

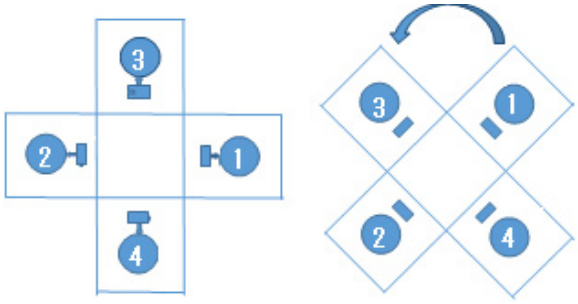

Fig. 14. Layout of servo motor for TMR.

Table 1. Specifications of QTRH.

Span of rotor		610 mm
Height		120 mm
Width		425 mm
Weight (including batteries)		1.41 kg
Battery	For motor	LiPo 3 cell (35 C, 2450 mAH)
	For radio control	LiPo 2 cell (25 C, 350 mAH)

Table 2. Specifications of TMR.

Rotor	APC Slow Flight: 11 × 4.7 inch
Motor	NTM 28-26: 1000 kV, 235 W
Servo motor	JR Propo DS359HV 3.5 kg-cm, 0.2 s/60°, 6 V
ESC	Turnigy Multistar 20 A

5.2. Implementation of Control System

We used Pixhawk (3D Robotics Inc.) as the flight controller, which controlled the attitude, altitude, and position of the airframe. Pixhawk employed an open architecture, and its circuitry and software are released publicly. The firmware consisted of an ArduCopter and Mission Planner (MP) installed on the ground PC. Pixhawk housed four types of sensors (three-axis gyro, three-axis accelerometer, three-axis magnetometer, and barometer) and used a GPS module. Various pieces of information regarding the flight controller were wirelessly transmitted to the ground PC at 10 Hz in real time, where the communication device employed an XBee module. The telemetry data transmitted by the flight controller were operated by the ground PC via the Mission Planner GUI to set various parameters, whereas the sensor information and control signals were recorded on the ground PC.

5.3. Implementation of Operating System

The radio control device consisted of a 14-channel transmitter (XG14, JR Propo) and 7-channel receiver (RG731BX, JR Propo). We employed seven channels: four for steering operation, two for TMR operation, and one for flight mode setting. The four TMRs had identical structures, which were arranged at 90° angle from each other (**Fig. 14**). The signals from the receiver to the servomotors were split into two and set in reverse, which was achieved using the XBus system (XB1-CV4, JR Propo), as presented in **Table 3**. In the skid mode, the steering operation of the operator was converted to a 45° vector by the radio control transmitter and then combined into signals for the two channels. The mixing settings for the radio control transmitter are listed in **Table 4**. To drive the servomotors in a stable manner, two batteries were mounted: one for control and the other for power.

Table 3. Servo motor name for TMR.

RC channel		Aux2	Aux3
Rotor axis		1–2 axis	3–4 axis
Rotor No.	1	XBus 7-1	
	2	XBus 9-1	
	3		XBus 7-2 (reverse)
	4		XBus 9-2 (reverse)

Table 4. Program mixing for RC transmitter.

Program No.	Primary > Secondary	High position [%] Low position [%]
1	Roll > 1–2 axis	Down −100 Up −100
2	Pitch > 3–4 axis	Left +100 Right +100
3	Pitch > 1–2 axis	Down +100 Up +100
4	Roll > 3–4 axis	Left +100 Right +100

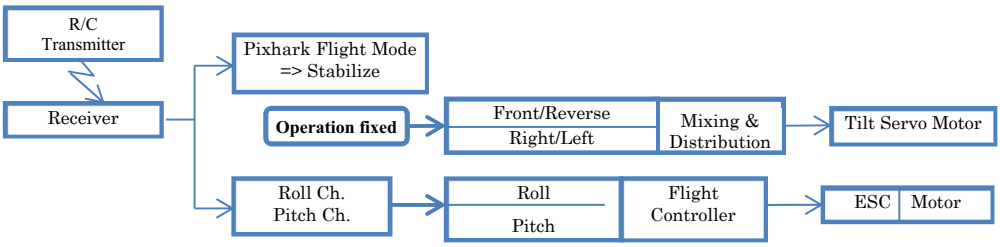

Fig. 15. Flow of normal mode.

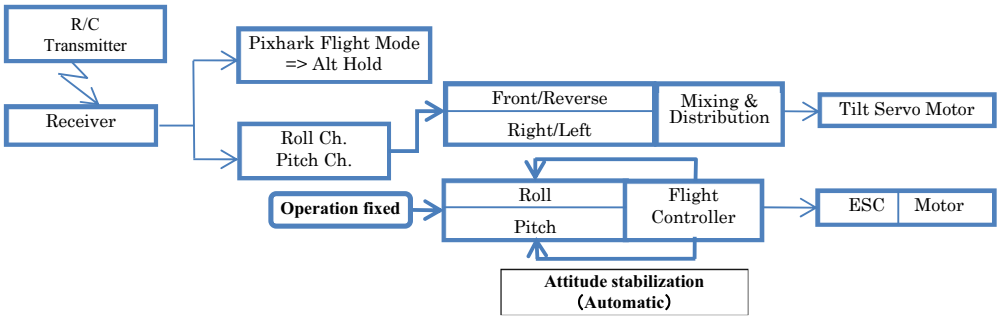

Fig. 16. Flow of skid mode.

5.4. Flight Mode

We prepared three flight modes that were switched from one mode to another as needed.

- Manual mode: used for takeoff and landing (control to stabilize attitude).
- Normal mode: used for the QRH (control to maintain altitude).
- Skid mode: TMRs were used (control to maintain altitude).

In this study, we employed the antiphase control of TMRs. The APM flight controller supports two types of automatic control: for stabilizing the attitude and for maintaining the altitude, which were used in the normal and skid modes. The control flows for the operation are shown in **Figs. 15** and **16**, and the steering system assignments are listed in **Table 5**.

The lift of the QTRH decreased according to the tilt angle when the TMRs were used. Therefore, the flight controller increased the speed of all the rotors to compensate for the lift loss. Furthermore, because crosswinds can be expected in outdoor environments, the QTRH thrust margin must be higher than that of conventional QRHs. For the TMRs of the experimental model, a thrust margin of approximately 1.3 times was used based on the compensation coefficient.

The robustness of the tilt mechanism and accuracy of the rotating system were important factors when implementing the TMRs, and the resonance due to the rotation of the rotors was monitored.

6. Test Flight

Although the test flights have been described previously [1, 2], we have added additional results and discussion to the earlier presentation in this paper.

Table 5. Operation in flight mode.

Operation item		Flight mode	
		Normal	Skid
QRH (Pixhark)	Roll, pitch	Stabilize	Alt hold
TMR (operator)	Forward/backward right/Left	Fixed servo motor	Tilting servo motor

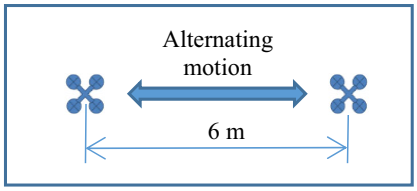

Fig. 17. Flight pattern of test flight 1.

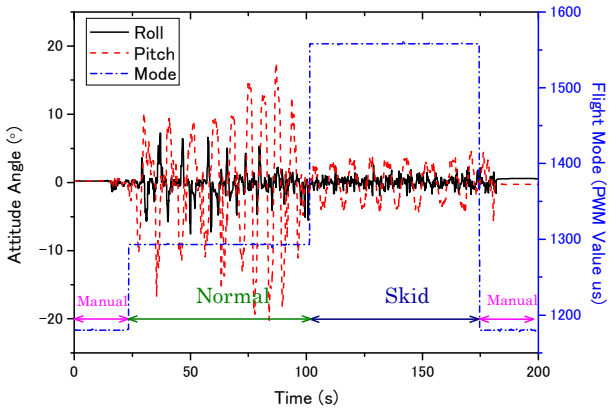

Fig. 18. Attitude angle of airframe in test flight 1.

6.1. Test Flight 1: Alternating Motion

The airframe flowed back and forth between two points 6 m apart at a constant speed and an altitude of 1.5 m. The attitude changes in the skid and normal modes were compared (**Fig. 17**). We expected significant changes in the attitude along the pitch axis.

The changes in the attitude angles for the roll, pitch, and angular velocity are shown in **Figs. 18** and **19**. The figures show pronounced effects on the pitch axis for both the attitude angles and angular velocity, as expected. The difference in attitude stability was pronounced at the turn points and was evident during steady (constant-speed forward) flight. The difference between the two flight modes was clear, and a quantitative comparison using standard deviations showed that the attitude angle was reduced to one-third and the angular velocity to two-thirds during the skid mode. These effects were also evident in the variations in the roll axis during the skid mode, where the results were better than the expected values. However, a slight tilting of the fore section during acceleration and downward tilting of the fore section during deceleration were observed. This is believed to be caused by the delayed response of Pixhawk's attitude stability control.

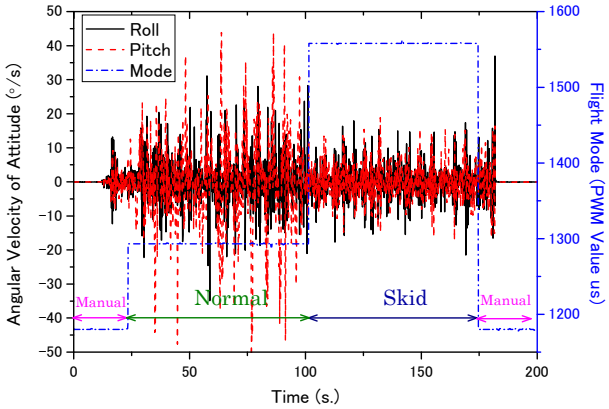

Fig. 19. Angular velocity of airframe in test flight 1.

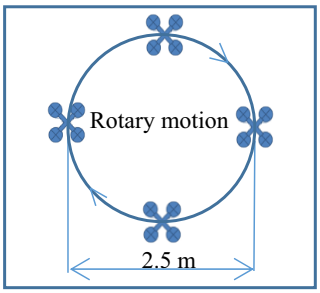

Fig. 20. Flight pattern of test flight 2.

6.2. Test Flight 2: Circular Motion

Keeping the fore section facing the same direction, the QTRH was flown to trace a 2.5 m-diameter circle at a constant speed and an altitude of 1.5 m. The attitude changes in the skid and normal modes were compared (**Fig. 20**). Attitude changes along the roll and pitch axes were expected to occur simultaneously.

The attitude angles about the roll and pitch axes and the angular velocity during test flight 2 are shown in **Figs. 21** and **22**, respectively. The expected effects were observed for both the attitude angle and the angular velocity of the airframe. The difference between the two flight modes was clear; quantitative comparisons using standard deviations showed that variations in the attitude angle were reduced to one-quarter, and those in the angular velocity were reduced to two-thirds. In the skid mode, the attitude angles about the orthogonal axes exhibited stable variations with a roughly 90° phase-angle difference, as expected. However, a slight tilting of the outer section of the circular flightpath was observed. This is believed to be caused by the delayed response of Pixhawk's attitude stability control.

6.3. Test Flight 3: Cross Wind Test

We observed the attitude stability when the airframe hovered in a crosswind generated by a large fan. This test flight was conducted indoors, where the distance between the fan and airframe was 2.5 m, the airframe altitude was 1.2 m, and the wind velocity was 4 m/s. The

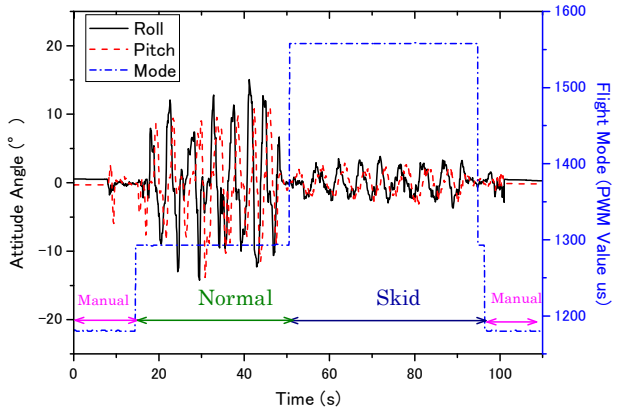

Fig. 21. Attitude angle of airframe in test flight 2.

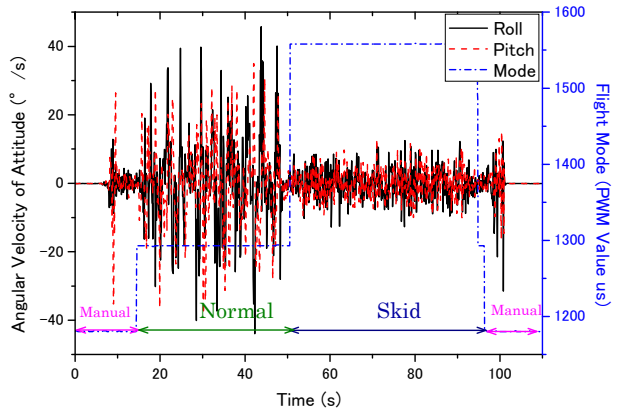

Fig. 22. Angular velocity of airframe in test flight 2.

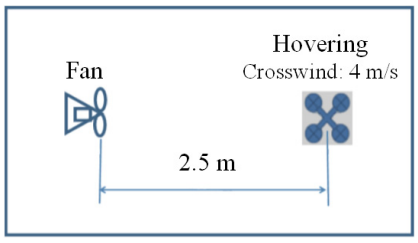

Fig. 23. Flight pattern of test flight 3.

Fig. 24. Scene of crosswind test (skid mode).

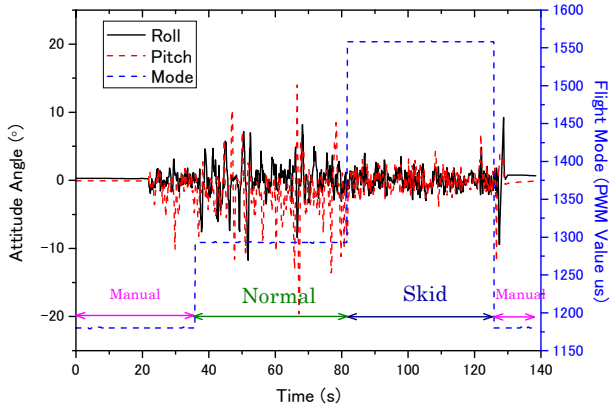

Fig. 25. Attitude angle of airframe in test flight 3.

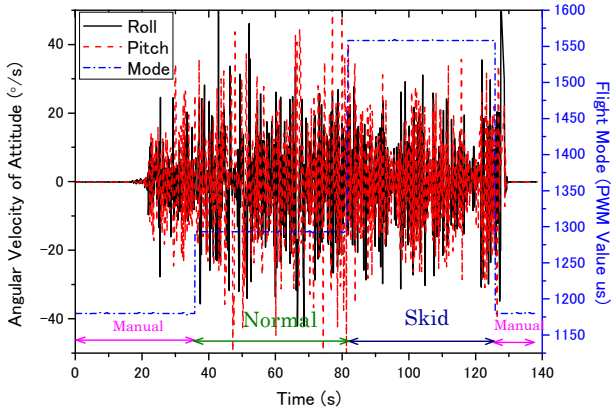

Fig. 26. Angular velocity of airframe in test flight 3.

attitude changes in the skid and normal modes were compared (**Figs. 23** and **24**, respectively). We expected that major attitude changes would occur along the pitch axis.

The changes in the attitude angle and angular velocity of the roll and pitch during test flight 3 are shown in **Figs. 25** and **26**, respectively. The figures show the presence/absence of downward tilting of the fore section and the high/low stability of the attitude toward the pitch axis in the two modes. However, the effect was not as clear as in the other test flights, and a quantitative comparison using standard deviations showed that the attitude angle was reduced to approximately 40% and the angular velocity to approximately 75% in the skid mode. The tilting down of the fore section occurred even in the skid mode, as shown in **Fig. 24**. The high/low attitude stability difference between the two modes occurred because, in the normal mode, the pitch axis was controlled to maintain the attitude, changing the front projection area, which then affected the aerodynamic drag, as shown in Eqs. (17) and (18).

7. Conclusions

Although the expected effects regarding the characteristics of maintaining a horizontal attitude were observed in all test flights, the following items need to improve.

1) Tilt up of fore section during acceleration

2) Tilt down of fore section during deceleration

3) Tilt down of outer side during circling

4) Tilt down of fore section in strong crosswinds

Although these aspects are slightly beyond the sensor capabilities of the proposed system, a certain degree of improvement can be expected by changing the flight controller settings. In item 4), a strong crosswind increases the relative velocity, which affects the aerodynamic drag computed by Eqs. (17) and (18).

As a software measure, we believe that adding feedforward control based on Eq. (9) to the thrust compensation should resolve the problem.

A possible hardware factor is the altitude maintenance function of the control system. In this system, we employed a barometer for altitude measurements, which was used for thrust compensation via PID control. It appears that the barometer altitude resolution (0.1 m) was the cause of the delayed response. This can be improved by adding an altimeter based on infrared light or ultrasonic waves.

8. Final Remarks

While verification tests have been given priority in previous reports of this study, this paper presents equations for translation and rotation based on Newton's method. The translation equation was validated based on the effect of the aerodynamic drag, as discussed in Section 6.3. However, we could not verify the validity of the rotation equation based on the test results. This paper presents a thrust compensation factor that depends on the tilt angle. We believe that the attitude stability can be further improved by applying this compensation factor to the feedforward transfer function of the skid-mode control system. It is also important to add a high-resolution altimeter with a faster response.

Acknowledgments

The author expresses his gratitude to Associate Professor Masafumi Miwa at Tokushima University for his advice in conducting this study.

References:

[1] A. Imamura, M. Miwa, and J. Hino, "Flight Characteristics of Quad Rotor Helicopter with Thrust Vectoring Equipment," J. Robot. Mechatron., Vol.28, No.3, pp. 334-342, 2016.

[2] A. Imamura, Y. Urashiri, M. Miwa, and J. Hino, "Flight Characteristics of Quad Rotor Helicopter with Tilting Rotor," The J. of Instrumentation, Automation and Systems, Vol.1, No.2, pp. 56-63, 2014.

[3] M. Ryll, H. H. Bülthoff, and P. R. Giordano, "Modeling and Control of a Quadrotor UAV with Tilting Propellers," 2012 IEEE Int. Conf. on Robotics and Automation, pp. 4606-4613, 2012.

[4] M. Ryll, H. H. Bülthoff, and P. R. Giordano, "First Flight Tests for a Quadrotor UAV with Tilting Propellers," 2013 IEEE Int. Conf. on Robotics and Automation, pp. 295-302, 2013.

[5] A. Imamura, M. Miwa, and J. Hino, "Level Maintenance of Quad Rotor Helicopter by Tilt Rotor Mechanism," Proc. of the 15th SICE System Integration Division Annual Conf. (SI2014), 3M1-3, 2014.

[6] A. Imamura and M. Miwa, "Fixed Altitude Control of Quad Rotor Helicopter with Tilting Rotor," Proc. of 46th Japan Society for Aeronautical and Space Sciences (JSASS) Annual Meeting, Article No.B24, 2015.

[7] A. Imamura and M. Miwa, "Modelling and Control of a Tilt Type Quad-Rotor Helicopter," Proc. of 47th Japan Society for Aeronautical and Space Sciences (JSASS) Annual Meeting, Article No.1B7, 2016.

[8] A. Imamura and M. Miwa, "Basis Study of Tilting Rotor Type Quadcopter – The Frame Construction of H Type and + Types Is Compared –," The Proc. of 2016 JSME Annual Conf. on Robotics and Mechatronics, Article No.1P1-17b4, 2016.

[9] A. Oosedo, S. Abiko, S. Narasaki, A. Kuno, and M. Uchiyama, "Position and Attitude Independent Flight Control of 4 Tilt Rotor UAV," Proc. of the 32nd Annual Conf. of the Robotics Society of Japan, Article No.RSJ2014AC3M1-01, 2014 (in Japanese).

[10] A. Oosedo, S. Abiko, A. Kuno, S. Narasaki, S. Kokubun, and A. Konno, "Pitch Up Hovering Flight Control of a Quad Tilt Rotor UAV," The Proc. of 2015 JSME Annual Conf. on Robotics and Mechatronics, Article No.2A1-G03, 2015 (in Japanese).

[11] M. Miwa, S. Uemura, and A. Imamura, "Arbitrary Attitude Hovering Control of Quad Tilt Rotor Helicopter," J. Robot. Mechatron., Vol.28, No.3, pp. 328-333, 2016.

[12] R. Akbar, B. Sumantri, H. Katayama, S. Sano, and N. Uchiyama, "Reduced-Order Observer Based Sliding Mode Control for a Quad-Rotor Helicopter," J. Robot. Mechatron., Vol.28, No.3, pp. 304-313, 2016.

[13] A. Imamura, M. Miwa, and J. Hino, "Flight Characteristics of a Quadrotor Helicopter Using Extra Deflecting Thrusters," The J. of Instrumentation, Automation and Systems, Vol.1, No.2, pp. 64-71, 2014.

[14] A. Imamura, S. Uemura, M. Miwa, and J. Hino, "Flight Characteristics of Quad Ducted Fan Helicopter with Thrust Vectoring Nozzles," The J. of Unmanned System Technology, Vol.2, No.1, pp. 54-61, 2014.

[15] K. Nonami, "Introduction to Drone Engineering – From Modeling to Control –," p. 61, Corona Publishing Co., Ltd., 2020 (in Japanese).

Supporting Online Materials:

[a] Soratamago, "Equations of Motion for Quadcopters," (in Japanese). https://okasho-engineer.com/quadcopter-motion-equation/ [Accessed June 16, 2021]

Name:
Akitaka Imamura

ORCID:
0000-0003-2899-5858

Affiliation:
Associate Professor, Osaka Sangyo University

Address:
3-1-1 Nakagaito, Daito, Osaka 574-8530, Japan

Brief Biographical History:

1987- Technical Instructor, Osaka Sangyo University
1993- Research Assistant, Osaka Sangyo University
2001- Assistant Professor, Osaka Sangyo University
2016- Associate Professor, Osaka Sangyo University

Main Works:

• "Flight Characteristics of Quad Rotor Helicopter with Thrust Vectoring Equipment," J. Robot. Mechatron., Vol.28, No.3, pp. 334-342, 2016.

Membership in Academic Societies:

• The Japan Society for Aeronautical and Space Sciences (JSASS)
• The Robotics Society of Japan (RSJ)
• The Society of Instrument and Control Engineers (SICE)
• The Japan Society of Mechanical Engineers (JSME)
• The Institute of Electronics, Information and Communication Engineers (IEICE)
• Institute of Electrical and Electronics Engineers (IEEE)